Synthesis and characterization of a new starch/SnO2 nanocomposite for efficient adsorption of toxic Hg2+ metal ion

Article *in* The Chemical Engineering Journal · April 2016

Impact Factor: 4.32 · DOI: 10.1016/j.cej.2016.04.084

9 authors, including:

Tansir Ahamad

King Saud University

82 PUBLICATIONS **485** CITATIONS

SEE PROFILE

Dr. Mohammad Mezbaul Alam

King Saud University

65 PUBLICATIONS **471** CITATIONS

SEE PROFILE

Zeid A Alothman

King Saud University

353 PUBLICATIONS **2,073** CITATIONS

SEE PROFILE

Chemical Engineering Journal 300 (2016) 306–316

Contents lists available at ScienceDirect

Chemical Engineering Journal

journal homepage: www.elsevier.com/locate/cej

Synthesis and characterization of a new starch/SnO_2 nanocomposite for efficient adsorption of toxic Hg^{2+} metal ion

Mu. Naushad [a,*], Tansir Ahamad [a], Gaurav Sharma [b], Ala'a H. Al-Muhtaseb [c,*], Ahmad B. Albadarin [d], Mohammad M. Alam [a], Zeid A. ALOthman [a], Saad M. Alshehri [a], Ayman A. Ghfar [a]

[a] Department of Chemistry, College of Science, Bld#5, King Saud University, Riyadh 11451, Saudi Arabia
[b] School of Chemistry, Shoolini University, Solan, Himachal Pradesh 173212, India
[c] Department of Petroleum and Chemical Engineering, Faculty of Engineering, Sultan Qaboos University, Muscat, Oman
[d] Bernal Institute, Department of Chemical and Environmental Sciences, University of Limerick, Ireland

HIGHLIGHTS

- Starch based nanocomposite (starch/SnO_2) was synthesized by sol–gel method.
- Starch/SnO_2 nanocomposite was used for the removal of Hg^{2+} from aqueous medium.
- The maximum adsorption capacity was found to be 333 mg g^{-1} at 25 °C.
- The adsorbed Hg^{2+} metal ion could be successfully desorbed using 0.1 M HCl solution.

GRAPHICAL ABSTRACT

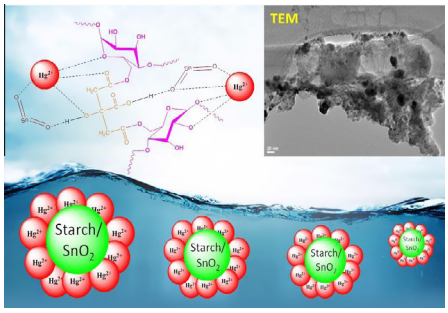

ARTICLE INFO

Article history:
Received 11 February 2016
Received in revised form 13 April 2016
Accepted 16 April 2016
Available online 22 April 2016

Keywords:
Starch/SnO_2 nanocomposite
Adsorption
Toxic metal ion
Kinetics
Regeneration

ABSTRACT

In this study, starch based nanocomposite (starch/SnO_2) was synthesized and used as an effective adsorbent for the removal of Hg^{2+} from aqueous medium. The as-prepared starch/SnO_2 nanocomposite was characterized by means of the XPS, XRD, BET, FTIR, SEM and TEM analyses. The effects of contact time, pH, initial Hg^{2+} concentration and temperature on the adsorption performance of starch/SnO_2 nanocomposite were investigated thoroughly. The experimental results showed that starch/SnO_2 nanocomposite had high ability to remove Hg^{2+} ion from aqueous medium. The adsorption of Hg^{2+} was maximum at the pH 6 and equilibrium was achieved within 60 min. The pseudo-second-order equation represented the adsorption kinetics with high correlation coefficient (>0.998) and the Freundlich isotherm model fitted the adsorption data better than the Langmuir. The maximum adsorption capacity was found to be 192 mg g^{-1} at 25 °C which was increased with the temperature, indicated the endothermic adsorption. The feasibility of Hg^{2+} adsorption onto starch/SnO_2 nanocomposite was also studied thermodynamically and the results showed that the adsorption was spontaneous and chemical in nature. The adsorption capacity of the regenerated adsorbents could still be maintained at 94% by the fourth adsorption–desorption cycle.

1. Introduction

The organic ion exchangers have been widely used for the treatment of wastewater but they have some limitations, like they

* Corresponding authors.
E-mail addresses: shad81@rediffmail.com (Mu. Naushad), almuhtasebala@gmail.com (A.H. Al-Muhtaseb).

http://dx.doi.org/10.1016/j.cej.2016.04.084
1385-8947/

are not thermally stable. Inorganic ion exchangers were also used as substitutes. Nevertheless, the inorganic ion exchangers also have their own restrictions, like they are not much more chemically stable and not suitable for column operation. Thus, the latest development in this field is to overcome these problems by fabricating the composites with suitable materials including, resins, agricultural residues, synthetic and natural polymers etc [1–5]. The combination of organic and inorganic precursors makes the composite materials which have high thermal and chemical stabilities. In designing composite materials, scientists and engineers have inventively combined various ceramics, metals and polymers to produce a new generation of outstanding materials that contain a wide variety of applications. Thus the synthesis of polymeric–inorganic composite has received a great deal of attention because it provided new material with special mechanical, chemical, electrochemical and optical as well as magnetic properties [6]. Many biopolymeric materials including pectin, cellulose, alginate, chitosan and gurgum etc have been thoroughly investigated by researchers for the synthesis of composite materials [7–9]. The starch is one of these biopolymeric materials found in nature in abundance with large number of functional groups present in its structure, thus making it choice of material to be explored for its vast applications. Starch is high molecular weight, nontoxic, inexpensive, biodegradable, having high surface area biopolymer which is easily extractable from natural plants [10,11]. These properties make it an excellent adsorbent for detoxification of hazardous pollutants from aqueous medium [12–15]. The presence of a large number of –OH groups in starch structure enhances its practical usability as these groups can be easily oxidized or reduced and also contribute in the formation of the ethers, esters or hydrogen bonds etc. The derivatization and crosslinking of starch increase its unique properties [16,17]. The usefulness of starch can be established by using it as potential adsorbent for heavy metal remediation [18]. The heavy metal pollution is most concerned topic of investigation in the present era due to its alarming rate of increase every day. Out of a number of toxic heavy metals, the upmost concern goes to mercury pollution.

The Hg^{2+} is a naturally occurring highly toxic metal which persist in environment for prolonged periods. The major sources of Hg^{2+} pollution results from human activities and has significantly increased the concentration of mercury ions in the surroundings over the past several decades. These activities includes industrial processes; as coal burning, chlorine production in the chlor-alkali industry, cement, zinc, steel and other metals manufacturing, incineration or dumping of mercury-containing products as biomedical waste, mining and product recycling etc [19–22]. The emitted Hg^{2+} ions get transformed into methylmercury a highly toxic compound which eventually builds up in water and soils and finally enters the food chain where it accumulates in the tissues of aquatic wildlife and moves to higher trophic levels including humans [23]. Thus, the addition of inorganic Hg^{2+} ions and there conversion to methylmercury, which occurs primarily in reducing zones in fresh aquatic bodies, terrestrial, coastal environments, and the subsurface ocean severely impacts the humans and wildlife [24]. The primarily human exposure to methylmercury results from eating of estuarine and marine fish [25]. The Hg^{2+} ions are highly neurotoxic in nature and also affect cardiovascular organs, kidney and bones etc [26–28]. Hence, the pre and post treatment of mercury waste is of immense importance in the context of environmental remediation.

The present study focuses on the synthesis of starch/SnO_2 nanocomposite and its potential application for the removal of toxic Hg^{2+} ions from aqueous medium. Adsorption equilibrium, thermodynamics and kinetic studies were also investigated.

2. Materials and methods

2.1. Synthesis of cross-linked starch dispersion

Dispersed solution of starch was prepared by mixing 3.0 g of starch in 100 mL of deionized water. For cross-linking the starch molecules, 3.0 g of citric acid (crosslinking agent) and 1.5 g of the catalyst $NaH_2PO_2{\cdot}H_2O$ were dissolved in the starch solution [29]. The starch suspension containing the crosslinking agent and catalyst was heated to 60 °C for 2 h with continuous stirring and then cooled to room temperature.

2.2. Synthesis of inorganic gel of SnO_2

0.1 M of tin (IV) chloride ($SnCl_4{\cdot}5H_2O$) solution was prepared by dissolving it in 4.0 M HCl solution. In a typical synthesis of SnO_2, the solution of NaOH (2.0 M) was added to 300 mL of the above solution drop-wise with controlled dropping rate for the chemical homogeneity until pH ~ 1. The resulting mixture was a whitish gel.

2.3. Synthesis of starch/SnO_2 nanocomposite

The starch/SnO_2 nanocomposite material was prepared by mixing the dispersed solution of cross-linked starch and the gel of SnO_2 with the continuous stirring and heating at 60 °C for 6 h [29]. The resultant opal gel was permitted to settle overnight at 25 °C. The supernatant liquid was decanted and the gel was filtered under suction and washed with 1.0 M HNO_3 to remove excess reagents. The excess acid was removed by washing with deionized water and then the composite material was dried in a hot air oven at 80 °C for several hours. The dry product was crushed into small granules of uniform size suitable for column separations/adsorption studies. They were then treated with excess of 1.0 M HNO_3 for 24 h at room temperature with occasional shaking, irregularly replacing the supernatant liquid with a fresh acid to certify the complete conversion of starch/SnO_2 nanocomposite into the H^+ form. The extra acid was removed after numerous washing with deionized water. The materials were finally dried at 50 °C in the oven, sieving to get particles of a particular size range (~125 μm) and kept in a desiccator.

2.4. Adsorption studies

Batch adsorption experiments were conducted in 250 mL conical flask by placing 100 mg starch/SnO_2 nanocomposite with 250 mL of 20 ppm Hg^{2+} solution at 25 °C and 150 rpm. The equilibrium study was performed by sampling at different time intervals (5–90 min) to achieve the equilibrium. The pH of the solution was adjusted using 0.1 M aqueous solutions of HCl/NaOH. Other parameters like temperature, pH and initial concentration of Hg^{2+} were also changed in order to optimize the adsorption process. After the adsorption process, starch/SnO_2 nanocomposite was separated from the solution and the concentration of Hg^{2+} in the aqueous phase was determined by atomic-absorption spectrophotometry.

The amount of Hg^{2+} adsorbed onto starch/SnO_2 nanocomposite, q_e was computed as follows:

$$q_e = \frac{V(C_o - C_e)}{W \times 1000} \quad (1)$$

where V is the volume of Hg^{2+} solution in litre, C_o and C_e are the initial and final concentrations (mg L^{-1}) of Hg^{2+} in solution, respectively, W is the weight (g) of starch/SnO_2 nanocomposite.

Isotherm and thermodynamic studies were also performed by varying the reaction temperature (25–50 °C) and initial concentration of Hg^{2+} solution (10–150 mg L^{-1}).

2.5. Desorption and regeneration studies

To be a good adsorbent, it should be reusable several times in adsorption–desorption cycles. In the present study, the desorption of Hg^{2+} was performed using 0.1 M aqueous solutions of HCl, H_2SO_4, HNO_3, CH_3COOH, and NaOH as the desorbing agents. The Hg^{2+} loaded starch/SnO_2 nanocomposite samples (100 mg) were kept in the 250 mL conical flask and shaken at 298 K for 60 min with the above desorbing agents (100 mL). Then the samples were separated from the solution, washed with deionized water and subjected again to adsorption–desorption process for four cycles. The metal recovery was calculated by the following equation [30]:

$$\%\text{Metal recovery} = \frac{\text{Amount of metal ions desorbed}}{\text{Amount of metal ions adsorbed}} \times 100 \qquad (2)$$

2.6. Antibacterial activity

The antibacterial activity of starch/SnO_2 nanocomposite was studied using standard optical density assay as described in previous studies [31,32]. One loopful of an overnight grown cultures of each *Staphylococcus aureus* or *Escherichia coli* was used as the inoculums and inoculated to 30 mL of sterile nutrient broth (NB) in a 100 mL Erlenmeyer flask, and these were incubated at 37 °C under continuous shaking for 24 h at 100 rpm. The culture was diluted to 10^5 colony forming units per mL with NB according to MacFarland standard. An aliquot of 10 mL of it was aseptically pipetted into a 190 mL NB in conical flasks. To the flask containing test organisms, the varying concentrations (50, 100, 150, and 200 μg mL^{-1}) of starch/SnO_2 nanocomposites were added. Then, again the flasks were incubated at 37 °C under continuous shaking for 24 h at 100 rpm. Aliquots of 4 mL were withdrawn at regular interval of one hour up to 24 h and optical density was measured at 620 nm. The positive control was also taken concurrently [33].

3. Result and discussion

3.1. Characterization of starch/SnO_2 nanocomposite

The surface area of starch/SnO_2 nanocomposite and Hg^{2+} adsorbed starch/SnO_2 nanocomposite was evaluated by Brunauer Emmett Teller (BET) equation [34] using Quantachrome surface area analyzer (USA) by N_2 adsorption at 77 K. The starch/SnO_2 nanocomposite showed the good surface area 11 $m^2\ g^{-1}$ which was decreased (78.5 $m^2\ g^{-1}$) after Hg^{2+} adsorption because some pores of starch/SnO_2 nanocomposite were closed due to the adsorption of Hg^{2+} onto starch/SnO_2 nanocomposite. The starch/SnO_2 nanocomposite material was prepared by mixing the dispersed solution of cross-linked starch and the gel of SnO_2 with the continuous stirring and heating at 60 °C for 6 h. The scheme of the synthesis is given in the Scheme 1. The FTIR spectra of starch, tin oxide and starch/SnO_2 nanocomposite are show in Fig. 1. In the spectra of starch and starch/SnO_2 nanocomposite, the peaks between at 3290–3380 cm^{-1} were corresponding to the –OH stretching vibrations in the starch [35,36]. The broadening in this region suggested the intermolecular hydrogen bonding. The presence of the methylene group was confirmed by the appearance of two strong bands at 2945–2830 cm^{-1} of νCH_2 *sym* and *asym* stretching and a band between 1480–1452 cm^{-1} was due to CH_2 bending mode. The characteristic peaks at around 1020 and 1210 cm^{-1} were attributed to the ether groups of the starch (C–O, stretching vibration). Another FTIR peak at 1635 cm^{-1} supported the presence of OH group (OH bending). The presence and the formation of ester groups after polymerization with citric acid were supported by the appearance of a FTIR bands at 1260 (m) cm^{-1}. The strong absorption band between 600–625 cm^{-1} attributed to the vibration of Sn–O–Sn groups. Furthermore, the wavenumber of the peak for Sn–O–Sn stretching vibrations shifted from its original position 650–625 cm^{-1}, which suggested that new interactions between starch molecules via hydrogen bonding into starch.

The morphologies and the particle sizes of SnO_2 in the nanocomposite were characterized by the TEM and HRTEM (Fig. 2a and b). The SnO_2 nanoparticles were agglomerated to the polymer matrix (starch) and the size of the SnO_2 nanocrystallines were in the range of 5–12 nm. The average diameter of the nanoparticles was found to be 8 nm. The HRTEM image of the selected nanocrystal of SnO_2 was inserted in Fig. 2b, and supported the crystalline nature of nanocrystals.

The distance between lattice fringes (d-spacing) were found to be 0.33 and 0.18 nm corresponding to the lattice spacing of 1 1 0 and 2 1 1 planes, these *hkl* vales were also supported with the XRD analytical results (Fig. 3), and indicated that nanoparticles were rutile SnO_2 structure and were well crystallized. The wide-angle *X-ray* diffractograms (WAXD) of the starch, SnO_2 and starch/SnO_2 nanocomposites are shown in Fig. 3. In the diffractogram of starch, three well defined peaks at 2θ, 16.68°, 17.92°, and 22.94° were observed, which corresponds to the typical crystal pattern of starch with miller indices (1 1 1), (2 0 0) and (2 1 1) respectively and indicated a semi-crystalline nature. The sharp and well-defined peaks appeared in the diffractogram of SnO_2 at 2θ, 26.880, 33.920, 37.990, 51.90, and 65.800 having miller indices (1 1 0), (1 0 1), (2 0 0), (2 1 1) and (3 0 1) indicated the planes of rutile SnO_2 crystallites, which were correlated with JCPDS reference data (JCPDS 41-1445) and were with good agreement of reported values. In the case of starch/SnO_2 nanocomposites, some peaks were disappeared and some became less intense which might be due to the presence of the polymer matrix and possible interaction. Although, the diffraction peak intensity of starch and SnO_2 in the starch/SnO_2 nanocomposite changed but there is no evidence of any additional peak or peak shift in the diffraction angles is observed that support only physical interaction between SnO_2 and starch. Therefore, it can be concluded that the diffractograms of starch/SnO_2 nanocomposites were only superimpositions of the diffractograms of the two components starch and SnO_2.

Over the past several decades, high resolution X-ray photoelectron spectroscopy has become very popular due to significant improvements in energy resolution that provide reliable information regarding the physico-chemistry of a material surface. The elemental composition was determined from survey scan. It was found that the starch/SnO_2 nanocomposite had carbon, oxygen and tin (Fig. 4a). The deconvolutions of the C1s regions of the spectra as shown in Fig. 4b, for the identification of the nanocomposite surface functionalities were fitted by six peaks, at 283.98, 284.24, 284.64, 258.41,286.48 and 288.47 eV corresponded to the carbon atom in the forms of C^*—C (sp^3), C^*—OH (primer and secondary), C—O—C^* (stretch ring), C—C^*=O (citric acid carbonyl), O=C^*—O—C (carbonyl group of ester), and C^*OOH (acidic group of citric acid unit), respectively. It was observed that the peaks of C—OH and C=O which belong to citric acid unit were slightly shifted to lower binding energy form its original position due to the polymeric nature of starch and interaction with SnO_2 in starch/SnO_2 nanocomposite. The O1s spectrum is also curve-fit using three peaks (Fig. 4c). The main peak at 531.54 eV was due to the presence of hydroxyl and ether groups. Small percentages of other types of O present at 530.52 eV can be attributed to various carbonyl (C=O) groups in the starch/SnO_2 nanocomposite. The resolved component corresponding to O1s at 531.0 eV belongs to SnO_2 structural oxygen atoms or oxygen inside non-stoichiometric oxides within the surface region of the material, while 532.7 eV corresponds to adsorbed oxygen and oxygen of the polymeric groups. The adsorbed oxygen exists on the grains or surface of the SnO_2

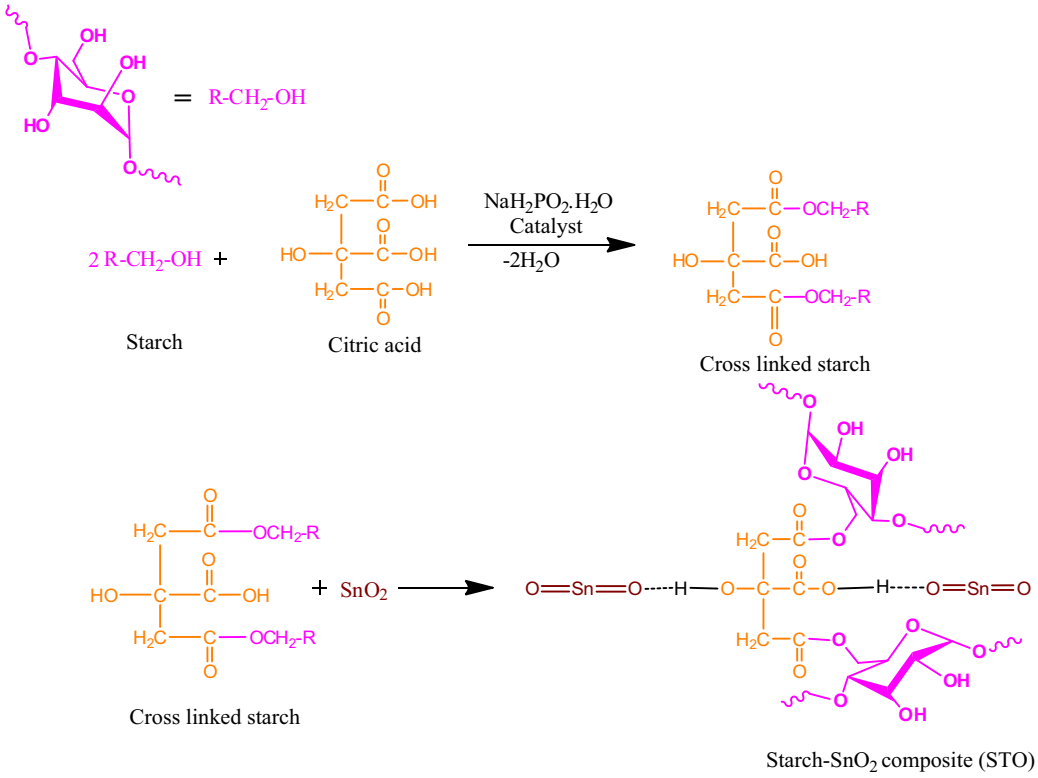

Scheme 1. Synthesis of starch/SnO_2 nanocomposite material.

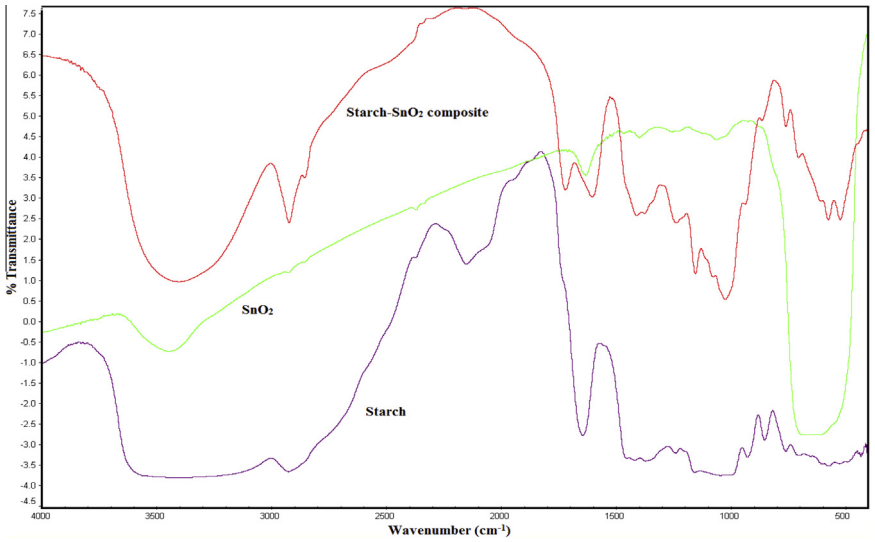

Fig. 1. FTIR spectra of starch, SnO_2 and starch/SnO_2 nanocomposite.

crystallites from O_2 molecules of the ambient atmosphere. As shown in Fig. 4d, the Sn3d high resolution spectrum that indicated two strong peaks belongs to $Sn3d_{5/2}$ and $Sn3d_{3/2}$ at 487.84 eV and 495.98 eV, respectively. It was observed that the binding energy of $Sn3d_{5/2}$ and $Sn3d_{3/2}$ was shifted to lower values that supported the interaction of SnO_2 with polymer matrix (starch) in the starch/SnO_2 nanocomposite. The adsorption of Hg^{2+} onto starch/SnO_2 nanocomposite was also supported using X-ray photoelectron spectroscopy (XPS). As shown in Figure a, the appearance of the Hg_{4d} and Hg_{4f} spectrum after the adsorption revealed that Hg^{2+} was adsorbed onto starch/SnO_2 nanocomposite. Two photoelectron peaks detected for $Hg_{4f7/2}$ (100.75 eV) and $Hg_{4f5/2}$ (104.80 eV) in the inset Figure (Figure a) implied that Hg^{2+} existed in a divalent state [37].

The SEM micrographs of starch/SnO_2 nanocomposite material at two different magnifications are given in Fig. 5a and b. It can be seen that the surface of starch/SnO_2 nanocomposite was porous and rough with cracking which might be due to the presence of crosslinked starch in the starch/SnO_2 nanocomposite.

3.2. Adsorption studies

The effect of contact time for Hg^{2+} adsorption using starch/SnO_2 nanocomposite material is shown in the Fig. S1. It was noted that

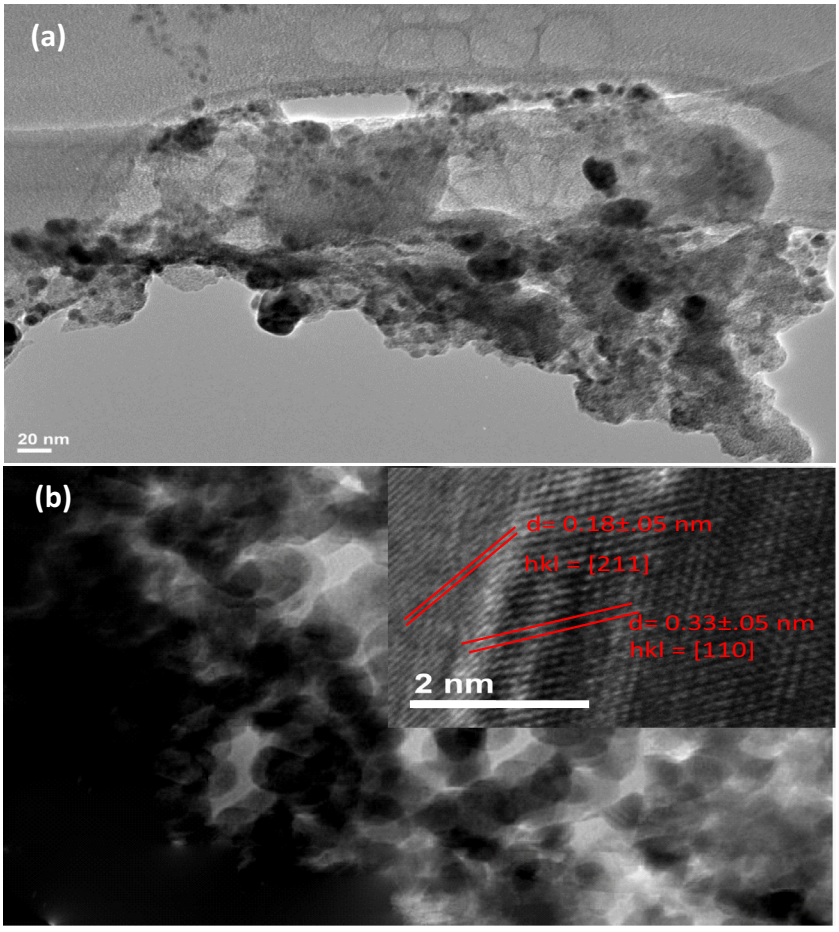

Fig. 2. (a) TEM of starch/SnO_2 nanocomposite (b) HRTEM of SnO_2 nanoparticles.

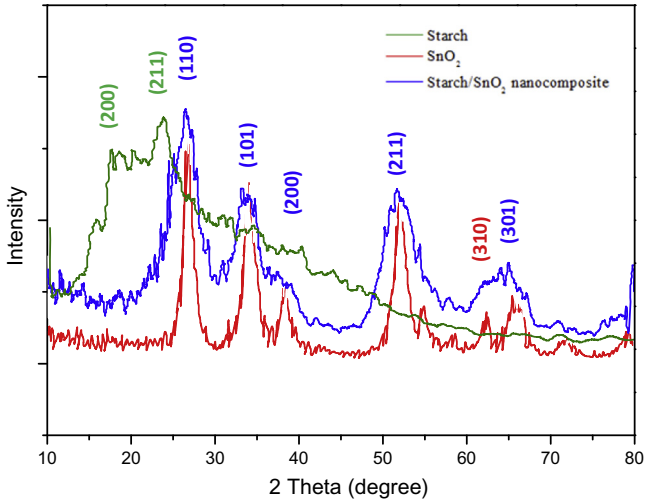

Fig. 3. XRD diffraction pattern of starch, SnO_2 and starch/SnO_2 nanocomposite.

the adsorption of Hg^{2+} was rapid at the initial stage and the equilibrium was achieved in 60 min. After, 60 min, there was no increment in the adsorption of Hg^{2+} metal ion. The rapid adsorption of Hg^{2+} metal ion at the initial stages was due to the accessibility of large number of vacant surface sites on the surface of starch/SnO_2 nanocomposite material [38]. The pH is an influential factor in the adsorption process which can affect the charge transfer between the solid and liquid. The effect of pH for the adsorption of Hg^{2+} onto starch/SnO_2 nanocomposite material was evaluated at different pHs which is shown in the Fig. S1. It was found that the removal efficiency was increased with increasing the pH. At pH 2, the adsorption was 42% which was increased to 95.5% at pH 6 and after that the adsorption started to decrease. The change in the adsorption efficiency with pH can be explained due to change in the ionic state of hydroxyl and carbonyl functional groups of starch/SnO_2 nanocomposite at different pH. In the acidic medium, the functional groups of starch/SnO_2 nanocomposite were protonated; as a result, the adsorption capacity of starch/SnO_2 nanocomposite to remove the Hg^{2+} metal ion was decreased. As the pH of the solution was increased, the hydroxyl and carbonyl groups were deprotonated and bonded with Hg^{2+} metal ions through electrostatic attraction [39]. The adsorption efficiency was decreased above the pH > 6. Therefore, all the following experiments were performed at a pH 6. The adsorption of Hg^{2+}onto starch/SnO_2 nanocomposite was also performed at different concentrations (10–150 mg L^{-1}) of Hg^{2+} metal ion where time and pH were kept 60 min and 6, respectively. It was noted that Hg^{2+} adsorption percentage was decreased from 99.5% to 72.5% with the increase in Hg^{2+}concentration from 10 to 150 mg L^{-1} (Fig. S1). This decrease in the adsorption percentage was due to the less availability of adsorption sites at the surface of starch/SnO_2 nanocomposite for the higher concentration of Hg^{2+} metal ion.

3.3. Reusability of starch/SnO_2 nanocomposite material

To reduce the cost of adsorption process for the practical application, the desorption of adsorbed Hg^{2+} from starch/SnO_2

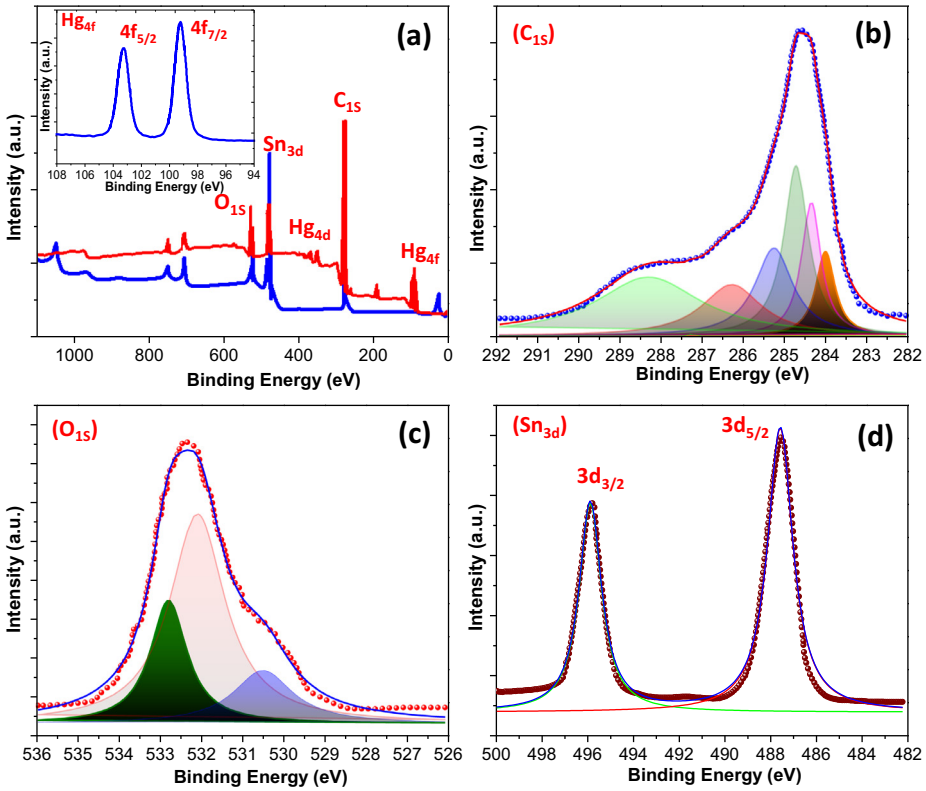

Fig. 4. X-ray photoelectron spectroscopic images (a) nanocomposite (inset figure shows the Hg^{2+} adsorption) (b) C1s (c) O1s (d) Sn3d.

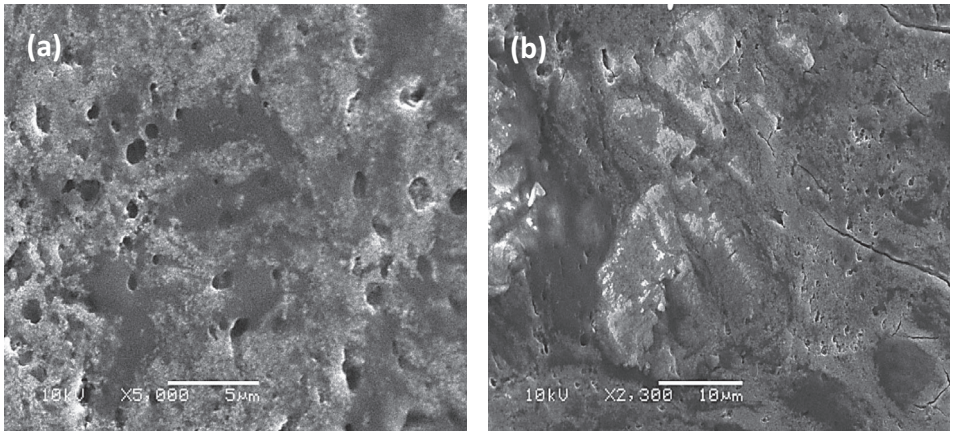

Fig. 5. SEM images of starch/SnO_2 nanocomposite at different magnifications.

nanocomposite and its regeneration is very important. It was noted that the desorption was maximum in 0.1 M HCl. The adsorbent was reused for four consecutive cycles, indicated a loss of only 2.5% in the adsorption percentage after four cycles which revealed a good regeneration capability of starch/SnO_2 nanocomposite material (Fig. 6a). Consequently, starch/SnO_2 nanocomposite could be economically and effectively used for the treatment of Hg^{2+} contaminated wastewater.

3.4. Rate constant study

In order to estimate the adsorption characteristic of starch/SnO_2 nanocomposite, it is important to investigate the rate at which Hg^{2+} toxic metal ion was removed from aqueous medium. Pseudo first-order and pseudo second-order kinetic models were applied.

3.4.1. The pseudo-first-order equation

The pseudo-first order equation of Lagergren [40] is generally expressed as:

$$\log(q_e - q_t) = \log q_e - \frac{k_1 t}{2.303} \tag{3}$$

where q_t and q_e are the amounts of Hg^{2+} adsorbed (mg/g) at time t, and at equilibrium, respectively, and k_1 is the rate constant of pseudo-first-order adsorption (1/min).

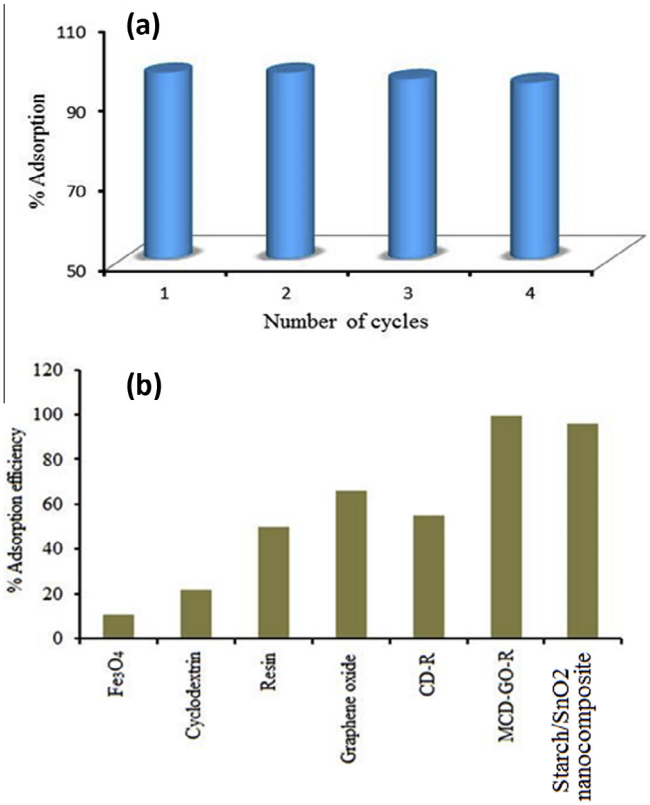

Fig. 6. (a) The adsorption efficiency of starch/SnO_2 nanocomposite in multiple adsorption/regeneration cycles. (b) Performance evaluations (wt = 8 mg, V = 25 mL, temp. 298 K).

The linearized form of the pseudo-first order model for the adsorption of Hg^{2+} metal ion onto starch/SnO_2 nanocomposite at various Hg^{2+} initial concentrations (20, 50 and 100 mg L^{-1}) is given in Fig. S2. The values of the rate constant k_1 were obtained from the slopes the plot of $\log(q_e - q_t)$ versus t (Table 1). The correlation coefficients values (R^2) for the pseudo first order kinetic model obtained at all the studied concentrations were low indicating that the adsorption of Hg^{2+} deviated significantly from the pseudo-first-order kinetic model.

3.4.2. The pseudo-second-order equation

The pseudo-second-order adsorption kinetic rate equation is expressed as [41]:

Table 3
Thermodynamics parameters for the adsorption of Hg^{2+} onto starch/SnO_2 nanocomposite.

Co, mg L^{-1}	$\Delta H°$, KJ mol^{-1}	$\Delta S°$, KJ mol^{-1} K^{-1}	$-\Delta G°$, KJ mol^{-1}		
			298 K	308 K	318 K
20	40.28	0.14	1.44	2.84	4.24

$$\frac{t}{q_t} = \frac{1}{k_2 q_e^2} + \frac{t}{q_e} \tag{4}$$

Where k_2 is the rate constant for the pseudo-second order adsorption (g/mg min).

The plots of t/q_t versus t of Eq. (4) gave linear plots (Fig. S2). The values of rate constant k_2 were evaluated from the intercepts of the plot (Table 1). The obtained values of the correlation coefficients (R^2) for pseudo-second-order kinetic model were >0.998 for all the studied concentrations. These results showed that the adsorption of Hg^{2+} onto starch/SnO_2 nanocomposite belongs to the pseudo-second-order kinetic model and Hg^{2+} was adsorbed on the surface of starch/SnO_2 nanocomposite via chemical interactions.

3.5. Adsorption isotherms

Adsorption isotherm studies are important to define the fraction of adsorbate molecules that are divided between solid and liquid phases at equilibrium. In the current study, the isotherm results were examined using the Langmuir and Freundlich isotherm models (Fig. S2).

According to the Langmuir, the uptake of adsorbate molecules takes place on a homogenous surface with a finite number of adsorption sites through monolayer adsorption without any interaction between adsorbed molecules. The linear form of the Langmuir isotherm model can be written as [42]:

$$\frac{1}{q_e} = \frac{1}{Q_m} + \frac{1}{bQ_m C_e} \tag{5}$$

where Q_m and b are the Langmuir constants related to maximum monolayer adsorption capacity and energy of adsorption, respectively. The values of Q_m and b were calculated from the intercept and slope of linear plots of $1/q_e$ vs. $1/C_e$, respectively (Table 2). It was found that the values of Q_m was increased with the increase in temperature which showed the endothermic nature of adsorption of Hg^{2+} onto starch/SnO_2 nanocomposite.

Table 1
Kinetic parameters for Hg^{2+} adsorption using starch/SnO_2 nanocomposite.

Initial concentration of Hg^{2+} (mg L^{-1})	Pseudo-first-order				Pseudo-second-order			
	Slope	Intercept	k_1 (min^{-1})	R^2	Slope	Intercept	k_2 (g mg^{-1} min^{-1})	R^2
20	−0.024	2.25	5.68×10^{-2}	0.935	0.019	0.13	2.86×10^{-3}	0.988
50	−0.025	1.95	5.75×10^{-2}	0.936	0.008	1.06	1.03×10^{-3}	0.988
100	−0.0255	1.55	5.87×10^{-2}	0.938	0.004	1.04	0.36×10^{-3}	0.987

Table 2
Langmuir and Freundlich adsorption isotherm constants for the adsorption of Hg^{2+} onto starch/SnO_2 nanocomposite.

Temperature (°C)	Langmuir constants				Freundlich constants			
	q_m (mg g^{-1})	b (L mg^{-1})	R_L	R^2	$1/n$	n	K_f	R^2
25	192	0.15	0.25	0.968	0.556	1.79	9.66	0.992
35	200	0.07	0.39	0.961	0.588	1.70	7.94	0.991
45	333	0.02	0.64	0.968	0.642	1.55	6.91	0.995

Table 4
List of various adsorbents (with maximum adsorption capacities) for the adsorption of Hg^{2+}.

Adsorbents	Maximum adsorption capacity (mg g^{-1})	References
Carboxymethyl-chitosan	280.8	[45]
Rice straw	27.7	[46]
Modified wool chelating fibers	43.3	[47]
Chitosan-phenylthiourea resin	135.5	[48]
Multi-walled carbon nanotubes	84.66	[49]
Magnetic mesoporous silica composites	1979	[50]
Silica	196.6	[51]
Polystyrene coated $CoFe_2O_4$ particles	86.9	[52]
Dowex-50 × -100	234.6	[53]
Silica-supported dithiocarbamate	80.2	[54]
GMA/DVB amine (R–N)	347	[55]
Dithiocarbamate chelating resin (DTMAN)	461.3	[56]
STO nanocomposite material	333	Present study

The essential characteristic of the Langmuir isotherm can be expressed in terms of the dimensionless equilibrium parameter R_L, which is defined as [43]:

$$R_L = \frac{1}{1 + bC_o} \tag{6}$$

where C_o (mg/L) is the lowest initial Hg^{2+} concentration and b is Langmuir constant (L/mg). The value of R_L indicates the type of the isotherm to be either unfavorable ($R_L > 1$), linear ($R_L = 1$), favorable ($0 < R_L < 1$) or irreversible ($R_L = 0$). In the present study the values of R_L was <1 which demonstrated the favorable adsorption of Hg^{2+} onto starch/SnO_2 nanocomposite.

The Freundlich isotherm is valuable to find the sorption phenomenon with the heterogonous sorbent media. This Freundlich isotherm is derived from the assumption that the sorption sites are disseminated exponentially with respect to the heat of sorption model. The linearized form of Freundlich isotherm is expressed by the following equation [44]:

$$\log q_e = \log K_f + \frac{1}{n} \ln C_e \tag{7}$$

where, K_f and n are the Freundlich adsorption constants which were determined from the intercept and slope of the linear plots of log q_e vs. log C_e, respectively.

The Langmuir and Freundlich parameters are listed in Table 2. The higher values of correlation coefficients ($R^2 > 0.998$) for Freundlich model than that of Langmuir model suggested multilayer rather than monolayer adsorption occurred onto starch/SnO_2 nanocomposite. Due to the lower value of correlation coefficient for the Langmuir isotherm model, this model could not properly described the relationship between the amounts of adsorbed Hg^{2+} metal ions and its equilibrium concentrations in the solutions.

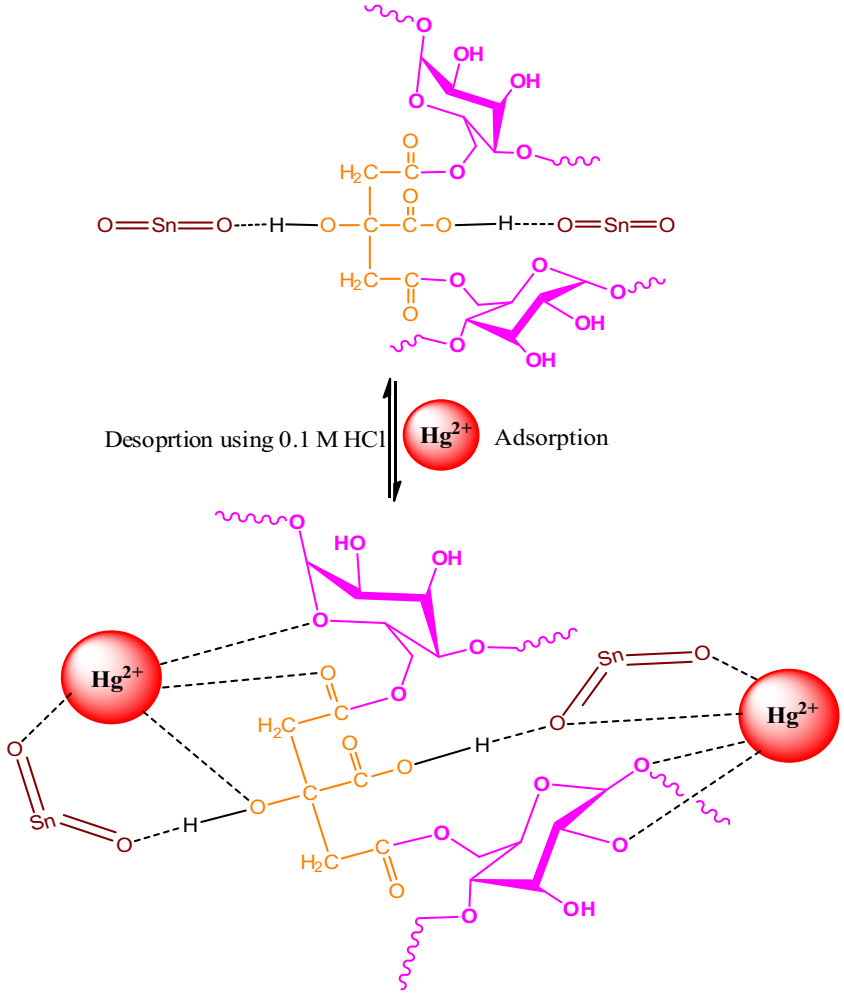

Fig. 7. Adsorption–desorption mechanism for Hg^{2+} ion using starch/SnO_2 nanocomposite.

3.6. Thermodynamic studies

Temperature has a distinct effect on the adsorption capacity of adsorbent. The adsorption of Hg^{2+} metal ion onto starch/SnO_2 nanocomposite was analyzed at different temperatures (25–50 °C). It was noted that the adsorption was increased with the increase of temperature which suggested the endothermic nature of the adsorption process (Fig. S1). The thermodynamic parameters, standard free energy change (ΔG°), standard enthalpy change (ΔH°) and standard entropy change (ΔS°) were evaluated to define the feasibility and nature of adsorption process. The values of ΔH° and ΔS° were calculated from the slopes and intercepts of the plots of ln K_c versus $1/T$ (Figure is not given) by using the following equation.

$$\ln K_c = -\frac{\Delta H^\circ}{RT} + \frac{\Delta S^\circ}{R} \quad (8)$$

The ΔG° (free energy change) was calculated from the following relation.

$$\Delta G^\circ = \Delta H^\circ - T\Delta S^\circ \quad (9)$$

where R (8.314 kJ/mol K) is the gas constant, T (K), absolute temperature and K_c (L/mg), standard thermodynamic equilibrium constant defined by q_e/C_e. The values of ΔG° and ΔH°, ΔS°, for Hg^{2+} adsorption onto starch/SnO_2 nanocomposite are given in Table 3. It is apparent from Table 3 that the values of ΔH° was positive indicated the endothermic nature of the adsorption. The positive values ΔS° revealed an increase in the randomness at the solid/solution interface during the adsorption process. The negative values of ΔG° indicated the degree of spontaneity of the adsorption process and ΔG° values were become more negative with the increase in temperature from 298 K to 318 K, showed that higher temperature favored the Hg^{2+} adsorption onto starch/SnO_2 nanocomposite.

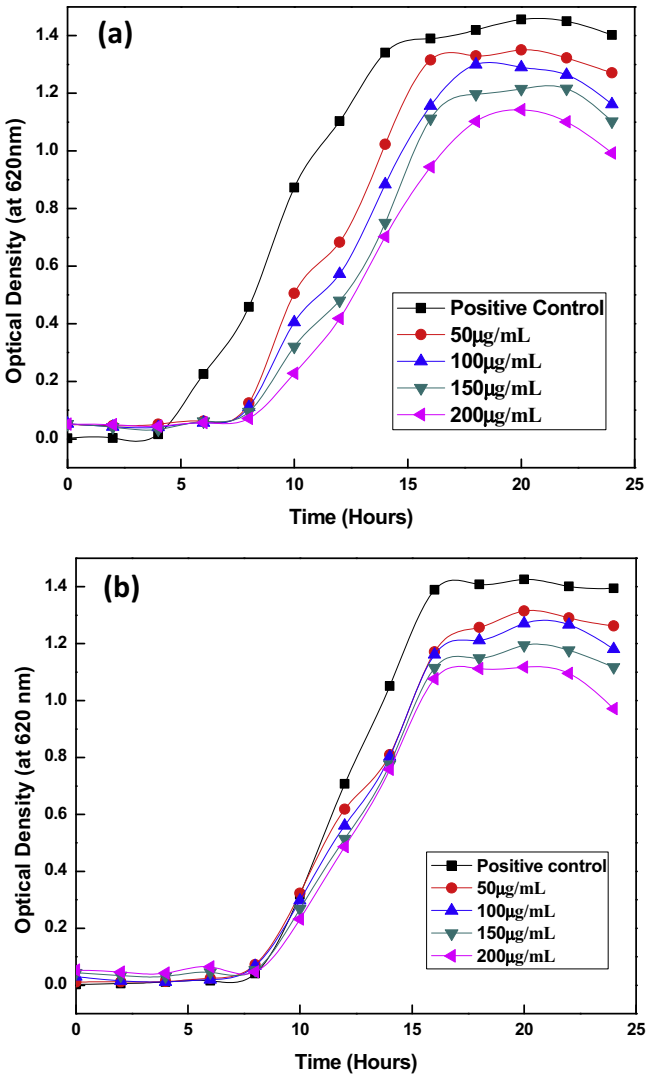

Fig. 8. Growth curves for (a) *Escherichia coli* and (b) *Staphylococcus aureus*.

3.7. Performance assessments

The maximum adsorption capacity of starch/SnO_2 nanocomposite was compared with the other adsorbents reported in the literature (Table 4) [45–56]. It was found that maximum adsorption capacity of starch/SnO_2 nanocomposite was higher than most of the adsorbents. Although, some adsorbents had better q_m than starch/SnO_2 nanocomposite, but they were expensive. So, on the basis of cost & performance, starch/SnO_2 nanocomposite had a better prospect. We had also assessed the performance of several adsorbents at the same conditions (adsorbent weight-8 mg; volume-25 mL and temperature 298 K). It was noted that starch/SnO_2 nanocomposite had better adsorption efficiency than Fe_3O_4, cyclodextrin, resin, graphene oxide and cyclodextrin sheet (CD-R) (Fig. 6b).

3.8. Adsorption/desorption mechanism

The proposed mechanism for the adsorption/desorption of Hg^{2+} metal ions onto starch/SnO_2 nanocomposite material is shown in Fig. 7. The starch/SnO_2 nanocomposite material had several carbonyl, hydroxyl and free oxygen groups. These groups are electron rich species and have tendency to donate the electron to the electropositive metal, according to the hard and soft acid base theory. Consequently, these groups were bonded to the Hg^{2+} metal ion through electrostatic attraction. The desorption of Hg^{2+} ion was performed using 0.1 M HCl. In the acidic medium, the functional groups of starch/SnO_2 nanocomposite were protonated; as a result, the adsorption capacity of starch/SnO_2 to remove the Hg^{2+} metal ion was decreased.

3.9. Antibacterial activity

The antibacterial nature of SnO_2/Starch composite was ascertained against two test organisms i.e., *S. aureus* and *E. coli* and it was found that the composite is effective against both the bacteria's. The SnO_2/Starch composite was an effective antimicrobial agent at all the concentrations as it inhibited the growth of *S. aureus* and *E. coli.* The concentration of 200 µg mL^{-1} was most effective against both *E. coli* and *S. aureus* (Fig. 8). The death phase of the test organisms was observed after 22 h of incubation. The presence of Sn metal in composite is accountable for its better antimicrobial activity. The mechanism may involve attachment of composite to the cellular membrane of the bacteria's, thus interfering in cellular activities such as active transport across cell membrane, retarding enzymatic activities and cell metabolism etc and ultimately causing cell lyses [57].

4. Conclusions

This study showed the successful synthesis of starch/SnO_2 nanocomposite material as an adsorbent for the removal of highly toxic Hg^{2+} metal ions from aqueous medium. The material was characterized by various analytical techniques and TEM analysis showed that the SnO_2 nanoparticles were agglomerated to the polymer matrix (starch) and the size of the SnO_2 nanocrystallines

were in the range of 5–12 nm. The maximum monolayer adsorption capacity was 333 mg g^{-1} and the removal percentage reached up to 97%. The kinetic studies denoted that the adsorption of Hg^{2+} metal ion onto starch/SnO_2 nanocomposite material followed pseudo-second order model and the equilibrium data fitted well Freundlich isotherm model. The thermodynamics results showed that the adsorption of Hg^{2+} onto starch/SnO_2 nanocomposite material was spontaneous and the reaction was endothermic. It was also found that the adsorbed Hg^{2+} metal ion could be successfully desorbed from the starch/SnO_2 nanocomposite material using 0.1 M HCl solution. The adsorption capacity of the regenerated adsorbents could still be maintained at 94% by the fourth adsorption–desorption cycle.

Acknowledgments

The authors would like to extend their sincere appreciation to the Deanship of Scientific Research at King Saud University for funding this work through the Research Group No. RG-1436-034. The authors are also thankful to the Sultan Qaboos University, Oman for the instrumental facilities for sample characterizations.

Appendix A. Supplementary data

Supplementary data associated with this article can be found, in the online version, at http://dx.doi.org/10.1016/j.cej.2016.04.084.

References

[1] D. Pathania, G. Sharma, A. Kumar, Mu. Naushad, S. Kalia, A. Sharma, Z.A. ALOthman, Combined sorptional-photocatalytic remediation of dyes by polyaniline Zr(IV) selenotungstophosphate nanocomposite, Toxicol. Environ. Chem. 97 (2015) 526–537.
[2] A. Kumar, D. Pathania, S. Kalia, M. Naushad, G. Sharma, Magnetically recoverable ZrO_2/Fe_3O_4/Chitosan nanomaterials for enhanced sunlight driven photoreduction of carcinogenic Cr (VI) and dechlorination & mineralization of 4-chlorophenol from waste water, RSC Adv. 6 (2016) 13251–13263.
[3] Mu. Naushad, Zeid A. Alothman, Separation of toxic Pb2+ metal from aqueous solution using strongly acidic cation-exchange resin: analytical applications for the removal of metal ions from pharmaceutical formulation, Desalin. Water Treat. 53 (2015) 2158–2166.
[4] A. Kumar, G. Sharma, M. Naushad, S. Thakur, SPION/β-cyclodextrin core-shell nanostructures for oil spill remediation and organic pollutant removal from waste water, Chem. Eng. J. 280 (2015) 175–187.
[5] G. Sharma, D. Pathania, M. Naushad, Preparation, characterization, and ion exchange behavior of nanocomposite polyaniline zirconium (IV) selenotungstophosphate for the separation of toxic metal ions, Ionics 21 (2015) 1045–1055.
[6] S.A. Nabi, Mu. Naushad, Synthesis, characterization and analytical applications of a new Composite cation exchanger cellulose acetate-Zr(IV) molybdophosphate, Colloids Surf. A 316 (2008) 217–225.
[7] S. Sharma, J. Kaur, G. Sharma, K.K. Thakur, G.S. Chauhan, K. Chauhan, Preparation and characterization of pH-responsive guar gum microspheres, Int. J. Biol. Macromol. 62 (2013) 636–641.
[8] D. Pathania, D. Gupta, N.C. Kothiyal, G. Sharma, G.E. Eldesoky, M. Naushad, Preparation of a novel chitosan-g-poly(acrylamide)/Zn nanocomposite hydrogel and its applications for controlled drug delivery of ofloxacin, Int. J. Biol. Macromol. 84 (2016) 340–348.
[9] A. Mittal, M. Naushad, G. Sharma, Z.A. ALothman, S.M. Wabaidur, M. Alam, Fabrication of MWCNTs/ThO_2 nanocomposite and its adsorption behavior for the removal of Pb(II) metal from aqueous medium, Desalin. Water Treat. (2015), http://dx.doi.org/10.1080/19443994.2015.1125805.
[10] V.P. Yuryev, A. Cesaro, W.J. Bergthaller (Eds.), Starch and Starch containing Origins-Structure, Properties and New Technologies Starch, Nova Science Publishers, Inc., New York, 2002.
[11] O.B. Wurzburg, in: O.B. Wurzburg (Ed.), Modified Starches: Properties and Uses, CRC Press, Boca Raton, 1986.
[12] B.S. Kim, S.T. Lim, Removal of heavy metal ions from water by cross-linked carboxymethyl corn starch, Carbohydr. Polym. 39 (1999) 217–223.
[13] D.K. Kweon, J.K. Choi, E.K. Kim, S.T. Lim, Adsorption of divalent metal ions by succinylated and oxidized corn starches, Carbohydr. Polym. 46 (2001) 171–177.
[14] S.M. Xu, S. Feng, G. Peng, J.D. Wang, A. Yushan, Removal of Pb (II) by crosslinked amphoteric starch containing the carboxymethyl group, Carbohydr. Polym. 60 (2005) 301–305.
[15] (a) M. Naushad, M.R. Khan, Z.A. ALOthman, I. AlSohaimi, F. Rodriguez-Reinoso, T.M. Turki, R. Ali, Removal of Br O_3^- from drinking water samples using newly developed agricultural waste-based activated carbon and its determination by ultra-performance liquid chromatography-mass spectrometry, Environ. Sci. Pollut. Res. 22 (2015) 15853–15865;
(b) M. Naushad, M.R. Khan, Z.A. AlOthman, M.R. Awual, Bromate removal from water samples using strongly basic anion exchange resin Amberlite IRA-400: kinetics, isotherms and thermodynamic studies, Desalin. Water Treat. 57 (2016) 5781–5788;
(c) M. Naushad, Z.A. ALOthman, M.R. Awual, M.M. Alam, Adsorption kinetics, isotherms, and thermodynamic studies for the adsorption of Pb^{2+} and Hg^{2+} metal ions from aqueous medium using Ti(IV) iodovanadate cation exchanger, Ionics 21 (2015) 2237–2245;
(d) M. Naushad, Z.A. ALOthman, Inamuddin, H. Javadian, Removal of Pb(II) from aqueous solution using ethylene diamine tetra acetic acid-Zr(IV) iodate composite cation exchanger: kinetics, isotherms and thermodynamic studies, J. Ind. Eng. Chem. 25 (2015) 35–41.
[16] G. Crini, Recent developments in polysaccharide-based materials used as adsorbents in wastewater treatment, Prog. Polym. Sci. 30 (2005) 38–70.
[17] K.B. Wesslen, B. Wesslen, Synthesis of amphiphilic amylose and starch derivatives, Carbohydr. Polym. 47 (2002) 303–311.
[18] R. Chandra, R. Rustgi, Biodegradable polymers, Prog. Polym. Sci. 23 (1998) 1273–1335.
[19] L. Wang, R. Xing, S. Liu, S. Cai, H. Yu, J. Feng, R. Li, P. Li, Synthesis and evaluation of a thiourea-modified chitosan derivative applied for adsorption of Hg(II) from synthetic wastewater, Int. J. Biol. Macromol. 46 (2010) 524–528.
[20] M. Xin, M.S. Gustin, D. Johnson, Laboratory investigation of the potential for re-emission of atmospherically derived Hg from soils, Environ. Sci. Technol. 41 (2007) 4946–4951.
[21] W.F. Fitzgerald, D.R. Engstrom, R.P. Mason, E.A. Nater, The case for atmospheric mercury contamination in remote areas, Environ. Sci. Technol. 32 (1998) 1–7.
[22] E.G. Pacyna, J.M. Pacyna, F. Steenhuisen, S. Wilson, Global anthropogenic mercury emission inventory for 2000, Atmos. Environ. 40 (2006) 4048–4063.
[23] M. Naushad, S. Vasudevan, G. Sharma, A. Kumar, Z.A. ALOthman, Adsorption kinetics, isotherms, and thermodynamic studies for Hg^{2+} adsorption from aqueous medium using alizarin red-S-loaded amberlite IRA-400 resin, Desalin. Water Treat. (2015), http://dx.doi.org/10.1080/19443994.2015.1090914.
[24] C.T. Driscoll, R.P. Mason, H.M. Chan, D.J. Jacob, N. Pirrone, Mercury as a global pollutant: sources, pathways, and effects, Environ. Sci. Technol. 47 (2013) 4967–4983.
[25] N.M. Lawson, P.R. Mason, Accumulation of mercury in estuarine food chains, Biogeochemistry 40 (1998) 235–247.
[26] O. Lindqvist, K. Johansson, M. Aastrup, A. Andersson, L. Bringmark, G. Hovsenius, L. Hakanson, A. Iverfeldt, M. Meili, B. Timm, Mercury in the Swedish environment, Water Air Soil Pollut. 55 (1991) 1–261.
[27] L.D. Hylander, M. Meili, 500 Years of mercury production: global annual inventory by region until 2000 and associated emissions, Sci. Total Environ. 304 (2003) 13–27.
[28] T.W. Clarkson, L. Magos, The toxicology of mercury and its chemical compounds, Crit. Rev. Toxicol. 36 (2006) 609–662.
[29] N. Reddy, Y. Yang, Citric acid cross-linking of starch films, Food Chem. 118 (2010) 702–711.
[30] A. Shahbazi, H. Younesi, A. Badiei, Batch and fixed-bed column adsorption of Cu(II), Pb(II) and Cd(II) from aqueous solution onto functionalised SBA-15 mesoporous silica, Can. J. Chem. Eng. 91 (2013) 739–750.
[31] G. Sharma, A. Kumar, M. Naushad, D. Pathania, M. Sillanpaa, Polyacrylamide@Zr(IV) vanadophosphate nanocomposite: ion exchange properties, antibacterial activity, and photocatalytic behavior, J. Ind. Eng. Chem. 33 (2016) 201–208.
[32] D. Pathania, G. Sharma, Mu. Naushad, A. Kumar, Synthesis and characterization of a new nanocomposite cation exchanger polyacrylamide Ce(IV) silicophosphate: Photocatalytic and antimicrobial applications, J. Ind. Eng. Chem. 20 (2014) 3596–3603.
[33] D. Pathania, G. Sharma, R. Thakur, Pectin@ zirconium (IV) silicophosphate nanocomposite ion exchanger: photo catalysis, heavy metal separation and antibacterial activity, Chem. Eng. J. 267 (2015) 235–244.
[34] S. Brunauer, P. Emmett, E. Teller, Adsorption of gases in multimolecular layers, J. Am. Chem. Soc. 60 (1938) 309–319.
[35] B. Shahrooie, L. Rajabi, A.A. Derakhshan, M. Keyhani, Fabrication, characterization and statistical investigation of a new starch-based hydrogel nanocomposite for ammonium adsorption, J. Taiwan Inst. Chem. Eng. 51 (2015) 201–215.
[36] M. Naushad, T. Ahamad, Z.A. Alothman, M.A. Shar, N.S. AlHokbany, S.M. Alshehri, Synthesis, characterization and application of curcumin formaldehyde resin for the removal of Cd^{2+} from wastewater: kinetics, isotherms and thermodynamic studies, J. Ind. Eng. Chem. 29 (2015) 78–86.
[37] Y. Wang, H. Yang, M. Pschenitza, R. Niessner, Y. Li, D. Knopp, A. Deng, Highly sensitive and specific determination of mercury(II) ion in water, food and cosmetic samples with an ELISA based on a novel monoclonal antibody, Anal. Bioanal. Chem. 403 (2012) 2519–2528.
[38] A.B. Albadarin, J. Mo, Y. Glocheux, S. Allen, G. Walker, C. Mangwandi, Preliminary investigation of mixed adsorbents for the removal of copper and methylene blue from aqueous solutions, Chem. Eng. J. 255 (2014) 525–534.
[39] L. Cui, Y. Wang, L. Gao, L. Hub, Q. Wei, B. Du, Removal of Hg(II) from aqueous solution by resin loaded magnetic b-cyclodextrin bead and graphene oxide sheet: synthesis, adsorption mechanism and separation properties, J. Colloid Interface Sci. 456 (2015) 42–49.

[40] S. Lagergren, About the theory of so called adsorption of soluble substances, Kungliga Svenska Vetenskapsakademiens Handlingar 24 (1898) 1–39.
[41] Y.S. Ho, G. McKay, Sorption of dye from aqueous solution by peat, Chem. Eng. J. 70 (1998) 115–124.
[42] I. Langmuir, The adsorption of gases on plane surfaces of glass, mica and platinum, J. Am. Chem. Soc. 40 (1918) 1361–1403.
[43] S.M. Alshehri, M. Naushad, T. Ahamad, Z.A. Alothman, A. Aldalbahi, Synthesis, characterization of curcumin based ecofriendly antimicrobial bio-adsorbent for the removal of phenol from aqueous medium, Chem. Eng. J. 254 (2014) 181–189.
[44] H.M.F. Freundlich, Over the adsorption in solution, J. Phys. Chem. 57 (1906) 385–470.
[45] S. Sun, A. Wang, Adsorption properties and mechanism of cross-linked carboxymethyl-chitosan resin with Zn(II) as template ion, React. Funct. Polym. 66 (2006) 819–826.
[46] C.G. Rocha, D.A.M. Zaia, R.V. da Silva Alfaya, A.A. da Silva Alfaya, Use of rice straw as biosorbent for removal of Cu(II), Zn(II), Cd(II) and Hg(II) ions in industrial effluents, J. Hazard. Mater. 166 (2009) 383–388.
[47] M. Monier, D.M. Ayad, A.A. Sarhan, Adsorption of Cu(II), Hg(II), and Ni(II) ions by modified natural wool chelating fibers, J. Hazard. Mater. 176 (2010) 348–355.
[48] M. Monier, D.A. Abdel-Latif, Preparation of cross-linked magnetic chitosan-phenylthiourea resin for adsorption of Hg(II), Cd(II) and Zn(II) ions from aqueous solutions, J. Hazard. Mater. 209–210 (2012) 240–249.
[49] M. Hadavifar, N. Bahramifar, H. Younesi, Q. Li, Adsorption of mercury ions from synthetic and real wastewater aqueous solution by functionalized multi-walled carbon nanotube with both amino and thiolated groups, Chem. Eng. J. 237 (2014) 217–228.
[50] B.Y. Song, Y. Eom, T.G. Lee, Removal and recovery of mercury from aqueous solution using magnetic silica nanocomposites, Appl. Surf. Sci. 257 (2011) 4754–4759.
[51] L.N.H. Arakaki, V.S. Augusto Filha, K.S. de Sousa, F.P. Aguiar, M.G. da Fonseca, J. G.P. Espınola, Silica gel ethyleneimine and its adsorption capacity for divalent Pb, Cd, and Hg, Thermochim. Acta 440 (2006) 176–180.
[52] K. Jainae, N. Sukpirom, S. Fuangswasdi, F. Unob, Adsorption of Hg(II) from aqueous solutions by thiol-functionalized polymer-coated magnetic particles, J. Ind. Eng. Chem. 23 (2015) 273–278.
[53] J. Tellinghuisen, Van't Hoff analysis of K°(T): how good or bad?, Biophys Chem. 120 (2006) 114–120.
[54] L. Bai, H. Hu, W. Fu, J. Wan, X. Cheng, L. Zhuge, L. Xiong, Q. Chen, Synthesis of a novel silica-supported dithiocarbamate adsorbent and its properties for the removal of heavy metal ions, J. Hazard. Mater. 195 (2011) 261–275.
[55] A.A. Atia, A.M. Donia, A.M. Yousif, Synthesis of amine and thio chelating resins and study of their interaction with zinc (II), cadmium (II) and mercury (II) ions in their aqueous solutions, React. Funct. Polym. 56 (2003) 75–82.
[56] A.F. Shaaban, D.A. Fadel, A.A. Mahmoud, M.A. Elkomy, S.M. Elbahy, Synthesis and characterization of dithiocarbamate chelating resin and its adsorption performance toward Hg(II), Cd(II) and Pb(II) by batch and fixed-bed column methods, J. Environ. Chem. Eng. 1 (2013) 208–217.
[57] S. Wadhwa, M. Bairagi, G. Bhatt, M. Panday, A. Porwal, Antimicrobial activity of essential oils of Trachyspermum ammi, Int. J. Pharm. Biol. Archives 1 (2010) 131–133.